Combustion and Flame 215 (2020) 86–92

Contents lists available at ScienceDirect

Combustion and Flame

journal homepage: www.elsevier.com/locate/combustflame

Combustion of 3D printed 90 wt% loading reinforced nanothermite

Jinpeng Shen[b,1,2], Haiyang Wang[a,1], Dylan J. Kline[a,b], Yong Yang[a,b], Xizheng Wang[b], Miles Rehwoldt[a,b], Tao Wu[b], Scott Holdren[b], Michael R. Zachariah[a,*]

[a] Department of Chemical and Environmental Engineering, University of California, Riverside, CA 92521, United States
[b] Department of Chemical and Biomolecular Engineering, University of Maryland, College Park, MD 20742, United States

ARTICLE INFO

Article history:
Received 4 November 2019
Revised 22 January 2020
Accepted 22 January 2020

Keywords:
Nanothermite
3D printing
Polymer hybrid
High loading
Mechanical properties

ABSTRACT

The use of Al-based nano-energetic materials has been limited in part due to difficulties in fabrication of high-density composites. In this paper, free-standing energetic composites with loading of up to 90 wt% Al-CuO were fabricated by 3D printing. A polymer hybrid of 3 wt% hydroxy propyl methyl cellulose (HPMC), 3.5 wt% nitrocellulose (NC) and 3.5 wt% polystyrene (PS), enables fabrication of mechanically strong and highly reactive composites. The energy flux can be readily tuned through the combustion speed and flame temperature by changing equivalence ratio. The highest energy flux was found to occur under fuel rich conditions (equivalence ratio = 2.4) which also corresponds to the maximum combustion speed (25 cm/s) despite the fact that the flame temperatures was lower. The Young's modulus of free-standing burn sticks was found to be as high as ~1 GPa, which is comparable to pure polypropylene. PS polymer flakes created during the high shear direct write process is believed to be critical to the enhanced mechanical properties we observed. The burning behavior using other oxidizers corresponds closely with that observed with mixed powders but with the added strength offered in a printed structure. This study offers an attractive route for safe, reliable and scalable additive manufacturing of Al-based nano-energetic materials at high energy densities.

1. Introduction

The combustion enthalpy of aluminum (Al) in oxygen is as high as 80 kJ/cm^3, which is substantially greater than those of monomolecular CHNO compounds (10–30 kJ/cm^3). [1–3] As a result, there is a growing interest in employing Al-based nano-energetic materials in propellants, explosives and pyrotechnics systems, such as additives in aerospace propellants, self-destructing microchips, etc. [1–7] This has also led to research in preparation methods, and, ignition and combustion mechanisms [8–13]. Assembly techniques include physical mixing [14], sol-gel [15], arrested reactive milling [16], layered deposition [17,18], electrospray [19], self-assembly [20], and metal organic frameworks (MOFs), and interface control techniques to improve the reactivity and energy output of nanothermites [21–24]. However, a main challenge moving forward is fabrication at high particle loading in order to obtain high energy density, without compromising the mechanical properties of the composite. Which is critical for the prevention of catastrophic failure in for example propellants [25–27].

Mechanical integrity is thus of significant importance for stable burning and potential real-world applications. Additive manufacturing techniques like 3D printing allows one to realize the fabrication from microscale to centimeter scale in a layer-by-layer manner, thus offering a customizability that is difficult to realize via conventional fabrication methods, leading to design and fabrication of multifunctional structures for a diverse range of applications [28–35]. Recent efforts in traditional energetic formulations include, Xu et al. [36] DNTF/NC/Viton composite explosives with a density of 1.785 g/cm^3. Li et al. [37] and Wang et al. [38] printed CL20-based composite explosive with low impact sensitivity and stable detonation properties. Chandru et al. [39] have developed a composite solid rocket propellant with customizable port geometries and controllable porosity and Driel et al. [40] prepared a TNO-base gun propellant using stereolithography 3D printing. By contrast the availability of Al-based energetic materials using 3D printing is very limited. Murray et al. [41] prepared Al-CuO nanothermites with 8 wt% solids loading by piezoelectric inkjet printing. Slocik et al. [42] created an energetic bio-thermite ink using ferritin liquid protein in water and Durban et al. [43] recently printed thermite with micron-size Al and CuO particles in an aqueous hydrogel matrix. However, in these studies [41–43], the

* Corresponding author.
E-mail address: mrz@engr.ucr.edu (M.R. Zachariah).
[1] J.P. Shen and H.Y. Wang contributed equally to this work.
[2] Present address: School of Chemical Engineering, Nanjing University of Science and Technology, Nanjing 210094, Jiangsu, China.

https://doi.org/10.1016/j.combustflame.2020.01.021
0010-2180/

a mechanical properties of these 3D-printed Al-CuO composites weren't reported. While these methods might be effective at designing and fabricating nano-thermite architectures, further advances might be limited due to shortcoming in scalability or poor stability from possible reactions between Al and water.

In our recent study, an Al-CuO nanothermite ink with particle loading as high as 90 wt% was developed for the first time by using a homogenous polymer mixture of polyvinylidene fluoride (PVDF, 4 wt%) and hydroxy propyl methyl cellulose (HPMC) (6 wt%) [44]. The burn rate of the printed sticks was ~2–10 cm/s, with burn temperatures of ~2800 K, and a Young's modules of ~0.3 GPa [44]. These materials were then interrogated by in-operando microscopy/thermometry to directly observe the phenomena of "reactive sintering" and the propagation of the reaction front [45–49].

In this study, we advance our prior work to create free-standing 90 wt% Al-CuO nanothermite sticks with Young's modulus of >1.0 GPa, and with higher reactivity with the addition of hydroxypropyl methylcellulose (HPMC), nitrocellulose (NC) and polystyrene (PS). Burn rates up to 25 cm/s were achieved, with flame temperature as high as ~2500 K. Other Al-based nanothermites with different oxidizers; Fe_3O_4, Co_3O_4 and WO_3 were also employed in this formulation. These results show that the 3D printing method using a hybrid binder strategy are well suited to a variety of Al-based nano-energetic materials yielding high reactivity and mechanical integrity.

2. Experimental

2.1. Materials

Aluminum nanoparticles (Al NPs, from Novacentrix Inc.) have an average diameter of 50–100 nm (TEM, Fig. S11a) with a ~2–5 nm oxide shell resulting in a ~81 wt% active Al content. CuO was purchased from US Research Nanomaterials. The particle diameter of nano-CuO are 80–200 nm (TEM, Fig. S11b). Dimethylformamide (DMF), Fe_3O_4, Co_3O_4, WO_3 and nitrocellulose (NC) (Collodion solution 4–8 wt% in ethanol/diethyl ether), Polystyrene (PS, average Mw: 280,000) were purchased from Sigma-Aldrich Corp. Hypromellose (METHOCEL^{TM}, HPMC, F4M Industrial Grade) was purchased from the Dow Chemical Company.

2.2. Ink preparation

HPMC (70.6 mg), NC (82.4 mg) and PS (82.4 mg) were mixed together to form hybrid polymer colloidal solution in 5 mL DMF using magnetic stirring for 4 h (Table S1). Nano Al and CuO (total mass of Al and CuO: 2117.7 mg) were then added into the colloidal solution and stirred with mechanical stirring for 2 h to form 3D printable colloidal ink. We explore Al-CuO mixtures with Φ values from 1.0 to 3.4 (Table S1). Other inks formulations with single or hybrid polymers (HPMC, NC and PS) or metallic oxide materials (Fe_3O_4, Co_3O_4 and WO_3) were prepared similarly (Tables S3 and S4, Fig. S1a and 1b).

2.3. Rheological characterization

The rheological properties of both the neat polymer solutions and the high particle loading inks were characterized by a Malvern Kinexus rheometer. The shear rates employed ranged from 0.01 to 100 s^{-1} at a fixed temperature of 25 °C, and the system was sealed to prevent possible solvent evaporation during the measurement. The details about the rheological property measurements could be found in our previous study [44].

2.4. Printing of colloidal inks

Printing was conducted with a Hyrel printer (SYSTEM 30 M) using a 0.9 mm inner diameter nozzle, and a substrate heating stage at 75 °C. Fig. S1c is schematic illustration of 3D printing of Al-CuO nano-thermite with HPMC-NC-PS hybrid polymers. The printing path was 8 cm × 8 cm at a feed rate of ~0.075 mL/min and a maximum write speed of ~22 cm/min. The ink was extruded through an 18 Gauge needle at a shear rate of rate ≈13 s^{-1} (≈4.5 mL/h). More details could be found in our previous studies [44,50].

2.5. SEM, TEM, FTIR, TG and XRD

The microstructure of films was investigated by using a Hitachi SU-70 SEM. The films were sectioned at low temperature by tweezers in liquid nitrogen and adhered to a carbon film on an SEM stage. TEM was conducted using JEOL JEM 2100 FEG. Attenuated total reflection (ATR) FTIR spectra of different polymer films without Al-CuO were collected using a Nicolet iS-50R spectrometer (Thermo Fisher Scientific) equipped with a room temperature deuterated triglycine sulfate (DTGS) detector FTIR spectroscopy. A Thermo Scientific Smart iTX accessory was installed to collect the ATR spectra shown here at 4 cm^{-1} resolution and averaged over 25 scans. TG results were obtained with a TA Instruments Q600 in an Ar flow (100 mL/min) at a heating rate of 10 °C/min. The crystal structures were characterized by XRD performed on a Bruker D8 diffractometer with Cu Kα radiation.

2.6. Combustion speed testing

Flame propagation was evaluated in an argon filled open-ended glass chamber. As is shown in Fig. S8, a Phantom v7 (Vision Research, Inc., Wayne, NJ) with a Nikon AF Nikkor 52 mm 1: 2.8 lens was used to record ignition and flame propagation of the composites and oriented perpendicular to the direction of flame propagation. The video rate was 7000 frames per second (fps) with a resolution of 256 × 128 pixels. The size of the sample is about 30 mm × 1.1 mm × 0.9 mm. Each experiment was repeated at least 3 times.

2.7. Flame temperature measurement

Color ratio pyrometry was performed using the same high-speed color camera. The details can be found in ref [51]. Briefly, three color ratios (green/red, blue/green, and blue/red) were simultaneously used to estimate temperature by minimizing their summed error from theoretical ratios with a nominal error less than ~110 K. For the figures that show temperature of a single sample as a function of time, only unsaturated pixels above the black level and within the error threshold are used to report mean/median temperature of the frame for a contiguous area of at least 10 acceptable pixels.

2.8. Mechanical testing

Tensile tests of the samples (30 layers) were performed using an INSTRON 3367 testing machine. Specimens were tested at a gage length of 10 mm and a cross-head speed of 5 mm/min. The Young's modulus was determined as the slope at low strain and the tensile strength was determined as the stress at specimen breakage. Compared to Al-CuO with HPMC-PS-NC hybrid polymers, tensile tests of the polymers (HPMC, NC, PS, HPMC-NC, HPMC-PS, NC-PS and HPMC-PS-NC) without Al-CuO were tested in the same condition (Table S6). Each experiment was repeated at least 3 times.

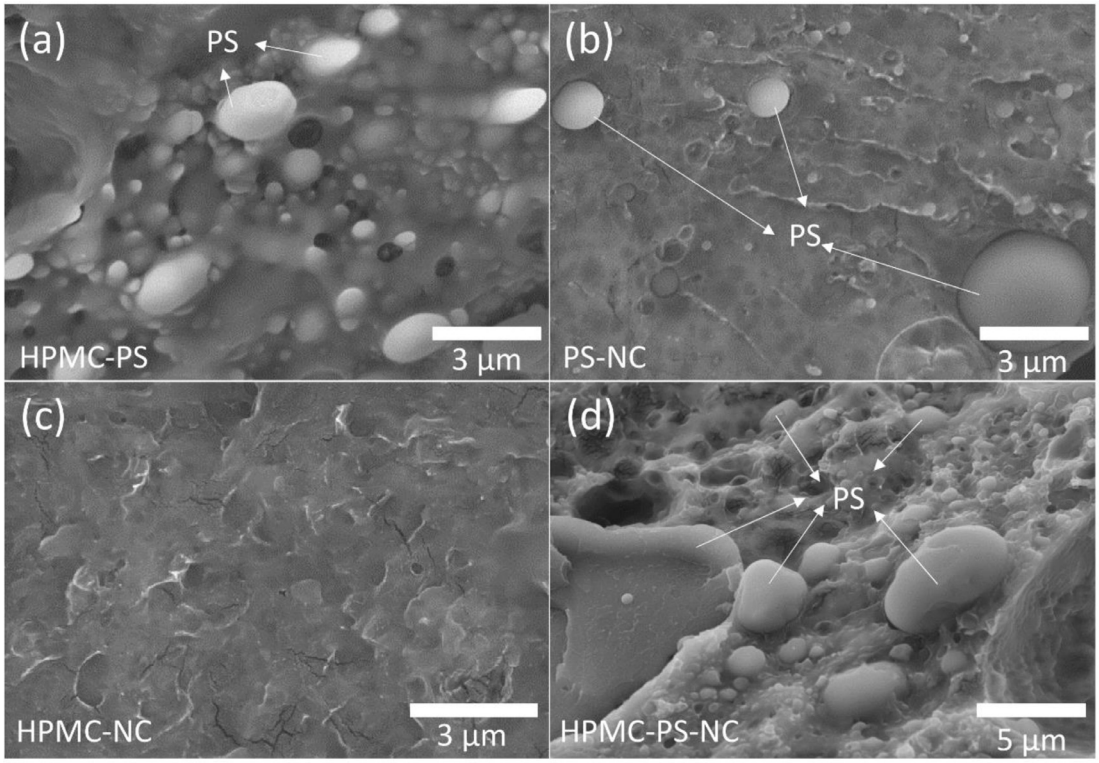

Fig. 1. Cross-sectional SEM images of different polymers hybrid (a: HPMC-PS; b: PS-NC; c: HPMC-NC; d: HPMC-PS-NC). Note: The low-resolution SEM images were shown in Fig. S3.

2.9. High-speed microscopy

As Fig. S10 shows, a 40x Nikon microscope objective with a working distance of 0.66 mm and an aperture of 0.75. The third port of the beamsplitter cube houses a red LED (630 nm), which is collimated using a plano convexlens at $1f$. The collimated beam is reflected by the beam splitter and focused on the sample via the microscope and the scattered light from the sample is imaged by the camera for focusing purposes. The high-speed video camera recorded at framerates of 18,000 frames/s, with an exposure of ~55 μs.

3. Results and discussion

3.1. Preparation of colloidal inks and morphology of the printed composite sticks

For any robust printing process, stability of composite inks is crucial for high quality 3D-printing, and the inks themselves should be resistant to phase separation over long periods of time. Using a polymer hybrid of 3 wt% hydroxy propyl methyl cellulose (HPMC), 3.5 wt% nitrocellulose (NC) and 3.5 wt% polystyrene (PS), a stable ink without any phase separation could be obtained (Figs. S1–S3). The introduction of NC was used to increase the flammability of the Al-CuO nanothermite due to its low ignition temperature. The addition of PS acts to reinforce the mechanical properties of the printed sticks since HPMC and NC have a relatively low Young's modulus of 0.62 GPa and 0.45 MPa, respectively, while PS is as high as 3.7 GPa, or 6x and 8000x higher than that of NC and HPMC [52–54].

Printing colloidal inks without nanoparticles show quite different morphologies, dependent on composition, as demonstrated in Fig. 1. All single-polymer cases had smooth, uniform surfaces in cross-section (Fig. S3), while all the hybrid-polymer cases were rough (Fig. 1a, b and d), with agglomerates in the cross-section (except for HPMC-NC, Fig. 1c). The spherical agglomerates on the rough surface are PS confirmed by energy dispersive spectrometer (EDS) point elemental analysis. It is also notable that in the HPMC-PS-NC case, some of the PS spheres were transformed into flakes (Fig. 1d), possibly because its inherent ductility results in shear induced morphological changes as it is injected through the syringe needle.

Addition of Al-CuO nanothermite into the formulations (see the procedure in Fig. S1), results in voids in all single-polymer samples, resulting in poor mechanical properties. The two-polymer hybrids were also eliminated from consideration since the inks suffer from phase separation (Figs. S2 and S4a). We were able to find however, an optimal formulation for the colloidal ink (Fig. S4b) at high loadings of 90 wt% Al-CuO, with three polymer mixtures (3.0 wt% HPMC, 3.5 wt% NC and 3.5 wt% PS). The homogeneity and composition of different inks with different polymer mixtures, and the morphology and quality of the corresponding printed samples were summarized in Table S1-S4.

The rheology of the ink and the possible interaction between different polymers were investigated, in order to better understand the need for the three-polymer blend. Fig. 2a shows shear viscosity of HPMC-PS-NC inks with and without Al-CuO nanothermites. Both pure polymer solutions and the composite ink show shear-thinning properties. Addition of the thermite dramatically increases the viscosity of the ink by approximately 1000x, but because these inks are extremely shear thinning, they approach the viscosity of the polymer at high shear rates. This property is ideal for a direct writing ink, enabling an otherwise high viscosity material to be pushed through a narrow nozzle [55]. Fourier transform infrared spectroscopy (FTIR) analysis (Fig. 2b and Table S5) provides insights into the possible interactions between HPMC, NC and PS. A clear shift (from 1632 cm^{-1} to 1644 cm^{-1}) of the NO_2 asymmetric stretching band (Fig. 2b) in HPMC–NC-PS composites compared to

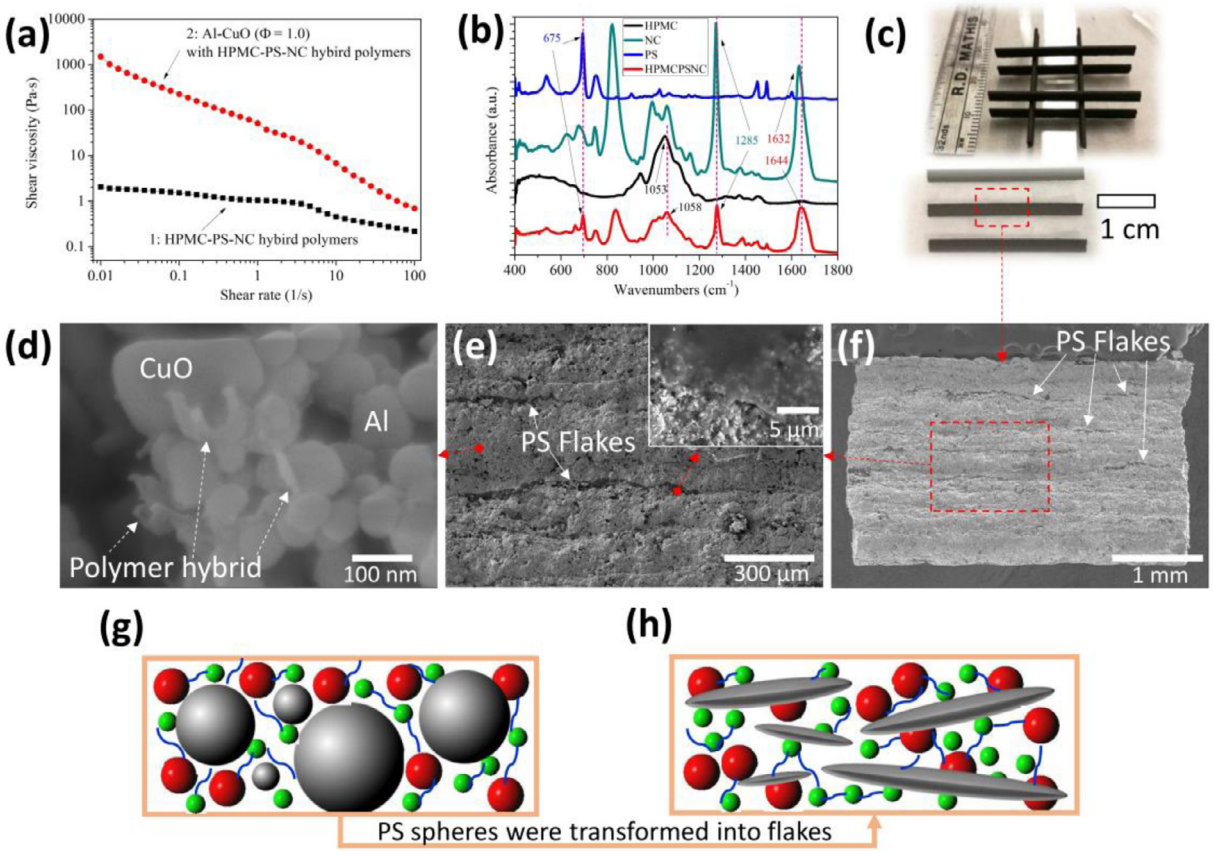

Fig. 2. (a) Apparent viscosity as a function of shear rate of line 1 (HPMC-PS-NC hybrid polymer solution) and line 2 (Al-CuO (Φ: 1.0) with HPMC-PS-NC hybrid polymer). (b) FTIR spectra of NC, HPMC, PS and HPMC-PS-NC hybrid polymers. (c) Photograph of the printed and stacked composites sticks (30 layers) with 90 wt% Al-CuO nano-thermite (equivalence ratio: 1.0) and 10 wt% HPMC-PS-NC hybrid polymer. (d) High magnification SEM image of the composite stick. (e) and (f) low magnification SEM images of the composite stick with PS flakes. The insert in (e) high magnification SEM image of PS flake. Schematic showing of the ink before (g) and after (h) extruding from the syringe, when the PS spheres were transformed into PS flakes.

pure NC, indicates possible hydrogen bonding between the NC and other polymers, and may provide enhanced interactions between nanoparticles [56].

Fig. 2c show the 30-layer composite sticks with 90 wt% Al-CuO nano-thermite (Equivalence ratio 1.0) and 10 wt% HPMC-PS-NC hybrid polymer (including 3.0 wt% HPMC, 3.5 wt% NC and 3.5 wt% PS), where the polymer content is confirmed by the TGA in Ar (Fig. S5). The inset SEM image shows the cross-sectional morphology of the composites.

Fig. 2d–f shows low and high magnification cross-sectional SEM images of 30 layers Al-CuO nanothermite composite sticks. The width and thickness of these sticks are ~ 0.9 mm and 2.3 mm, respectively. As the high magnification SEM image (Fig. 2d) shows, hybrid polymer particles of ~20 nm are observed among the Al-CuO nanothermites. Our previous study [44] showed that polymer gelation upon heating plays a critical role in enabling the formation of free-standing structures with minimal binder (<10%). The high magnification SEM image and EDS results also show close assembly between Al and CuO nanoparticles (Fig. S6).

The architecture of the energetic materials plays a significant role in the mechanical properties and reactivity [57–59]. As seen in Fig. 2e and f, polymer flakes in ~μm thickness and ~mm length observed among different layers with a spacing of ~100–300 μm were confirmed to be PS. As we mentioned above, owing to its low glass transition temperature (~100 °C), polystyrene (PS) is easily transformed upon heating. When extruding PS spheres containing ink from the thin syringe needle to the pre-heated substrate (~75 °C), the PS spheres (Fig. 2g) were transformed into PS flakes (Fig. 2h) by shear. The PS flakes are likely responsible for the significant improvement in mechanical behavior observed as discussed below.

3.2. Mechanical properties of the printed composite sticks

Mechanical properties were found to be independent of equivalence ratio, thus independent on particle type (from 1.0 to 3.4), with the tensile strength and modulus of the composite roughly constant at ~5 MPa (Fig. 3a) and 1 GPa (Fig. 3b). Compared to the particle-free hybrid polymers (Fig. 3 and Table S6), the particle containing composites show a 10x decrease in tensile strength, however the Young's modulus shows a modest decline. Keep in mind that we are dealing with a 90 wt% particle loading composite so this result is a significant improvement over what has been achieved for comparable samples using 3D printing approaches [41–43]. For reference, Fig. S7a–d shows stress-strain curves, tensile strength and Young's modulus for the different pure polymers of HPMC, NC and PS, as well as different hybrid polymers.

3.3. Combustion performance of printed composites

The burn rate and flame temperature of the composite sticks for equivalence ratios of 1.0 to 3.4 in Ar (1 atm) were obtained by high-speed color camera pyrometry [51] (Fig. S8). Typical burning snapshots of the composites at an equivalence ratio of 1.0 and 2.4 are shown in Fig. 4a and b, and the other results are summarized in Table S7. It is clear that propagation is stable in both cases, with the rich (Ø = 2.4) case observed to have a larger and brighter

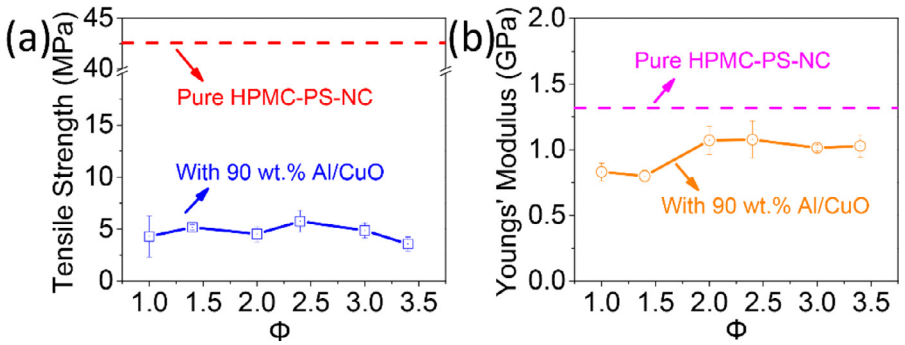

Fig. 3. Tensile strength (a) and Young's modulus (b) of 90 wt% Al-CuO with 10 wt% HPMC-PS-NC hybrid polymers (3.0 wt% HPMC, 3.5 wt% NC and 3.5 wt% PS) as a function of equivalence ratio. Inset horizontal dashed lines are tensile strength and Young's modulus of HPMC-PS-NC hybrid polymers, respectively.

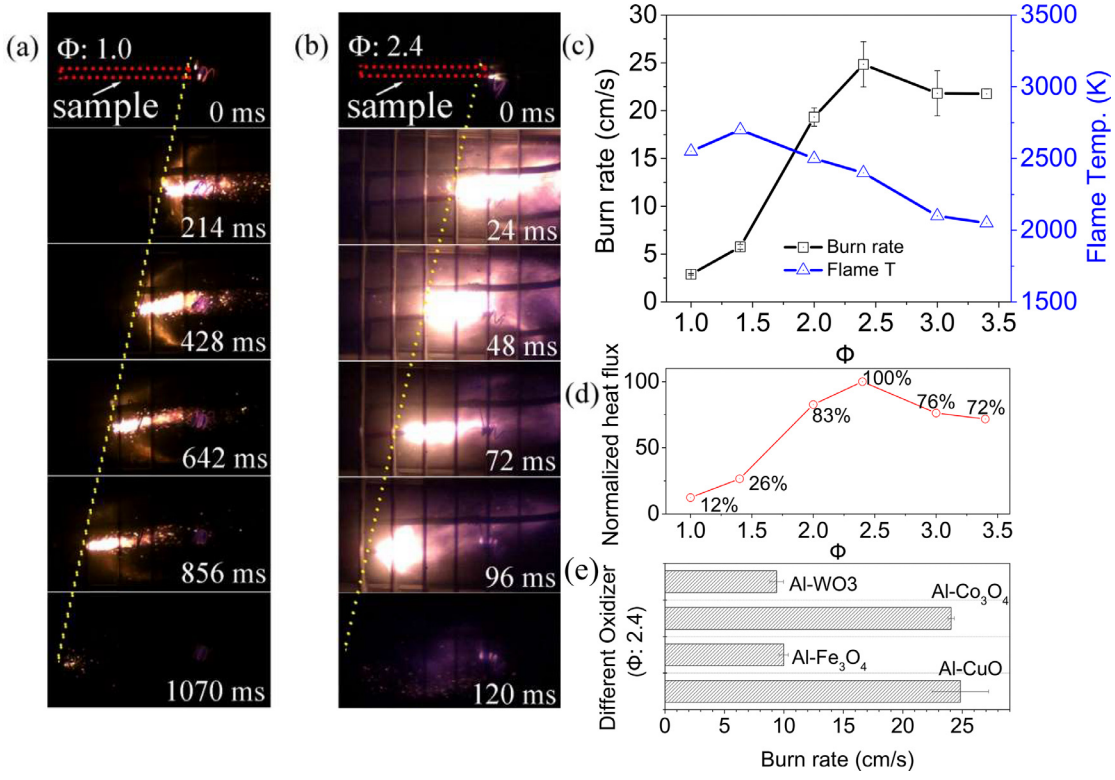

Fig. 4. Temporal combustion snapshots of the composites at equivalence ratio of 1.0 (a) and 2.4 (b) in Ar. (c) Burn rate and flame temperature of 90 wt% Al-CuO with 10 wt% HPMC-PS-NC hybrid polymers at equivalence ratio from 1.0 to 3.4. (d) Normalized heat flux of composites sticks with different equivalence ratios. (e) Burn rate of Al with various oxidizers printed under the same conditions (15 layers). Note: Relative Heat flux = burn rate × flame temperature × density × cross-sectional area. The apparent densities of the composite sticks are shown in Fig. S12.

flame compared to the stoichiometric case (anerobic conditions). Burn rate also peaks at the rich side (Ø = 2.4) at a velocity of ~25 cm/s (Fig. 4c). Flame temperature is also plotted in the same figure and shows a gradual decrease from 2600 K to 2100 K (Table S7), which we attribute to the combustion products transition from Cu and Al_2O_3 to a mixture of Al_2O_3, Al_4Cu_9 and Al_2Cu according to X-ray diffraction results (Fig. S9) [60]. Given the burn rate increases by 10x when increasing the equivalence ratio from 1.0 to 2.4, while the flame temperature only has a ~400 K decrease, results in a normalized heat flux that also peaks at an equivalence ratio of 2.4, and is ~8x the stoichiometric case (see Fig. 4d). Thus, operating rich has significant performance gains, but also suggest that combustion of the fuel is likely kinetically limited.

To confirm that the method is applicable to other oxidizers, composites of Al-CuO, Al-Fe_3O_4, Al-Co_3O_4 and Al-WO_3 at equivalence ratio of 2.4 were also printed and the combustion propagation speed shown in Fig. 4e. Burn rates with different oxidizers show results consistent with raw powder samples physically mixed and ignited in a combustion cell. This is not surprising since our composite sticks are essentially pure thermite mixtures (i.e. 10 wt% binder) [61,62].

3.4. Probing the flame front

Reactive sintering plays a significant role in nanothermite combustion by rapidly coalescing aggregated NPs, and thus increasing the effective size of the particles before reaction (sintering ≤ reaction time) [19,50,63]. We recently directly observed this significant phenomenon with high temporal and spatial resolution by using a microscope coupled high-speed camera [50]. These results showed post-reactive sintering size, and flame thickness of ~20 μm and ~30 μm, respectively.

The *in-operando* high-speed microscopy imaging was also used in this study to probe the flame front of the Al/CuO/HPMC/NC/PS

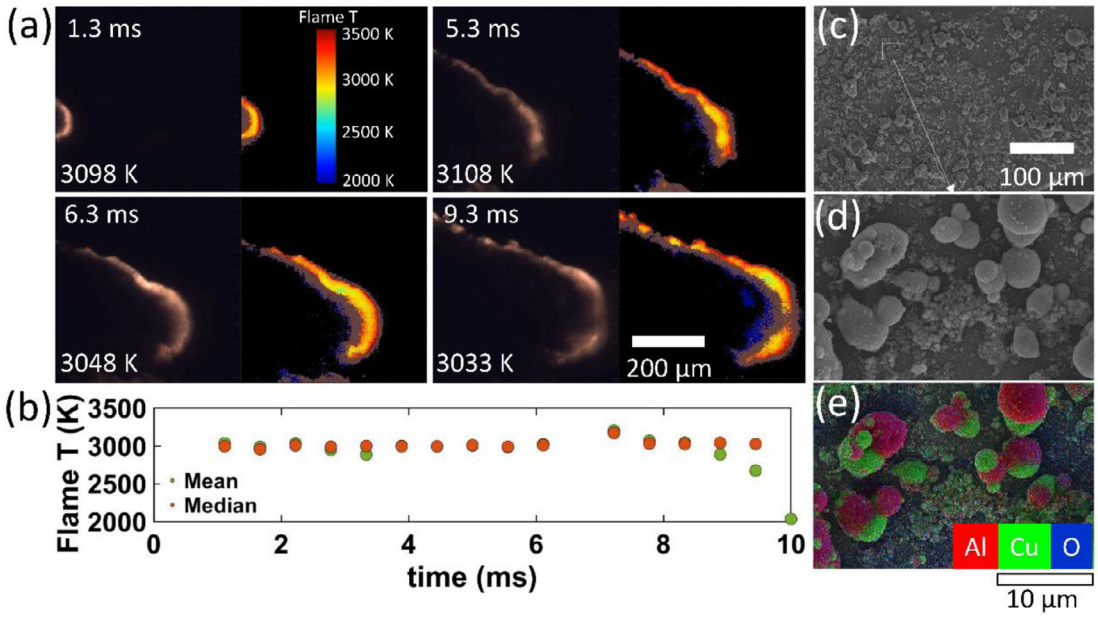

Fig. 5. Flame propagation and the corresponding flame temperature map obtained by in-operando microscopy/thermometry (a) temperature profile (b)temperature as a function of time. The low (c) and higher resolution (d) SEM image and its corresponding EDS mapping results (e) of the post-combustion products.

(90 wt% Al-CuO; Ø = 1.0). The experimental configuration is shown in Fig. S10 and has been discussed in detail elsewhere [50]. Fig. 5a shows the temporal flame propagation snapshots with a scale of ~512 µm × ~512 µm and a resolution of ~1 µm/pixel along with the resulting color pyrometry temperature as previously described [50]. The flame front images and corresponding temperatures are shown in Fig. 5b. The mean flame front temperature of the printed Al/CuO/HPMC/NC/PS (90 wt% Al-CuO) was measured to be ~3000 K with a flame front thickness ~30 µm (Fig. 5a), which is ~400 K higher than that in Fig. 4c. We attribute this difference to the length scale and location of view. A temperature of ~2600 K (Fig. 4c) was measured based on the macroscope view (~3 cm) of the whole burning stick (also including cooling products), while under microscopic conditions which imaged only the hot reaction front we see temperature ~3000 K. The latter result based on the thickness of the front a thermal gradient of ~10^6 K/cm. If we consider from the image we see the reaction front is at most 50 µm, and with a velocity ~ 5 cm/s (Ø = 1.0) leads to heating rates of 10^7–10^8 K/s and reaction times of ~ 1 ms. These results are very consistent with our prior study of Al/CuO/HPMC/PVDF [50]. The resulting sintered particle size from post-combustion analysis shows particles in the (Fig. 5c) ~2–20 µm range which is roughly the same as that seen for Al-CuO nanothermites powders [19]. Higher resolution SEM image and its EDS result are shown in Fig. 5d and e, respectively. The post-combustion products show a common "snowman" structure in which Al_2O_3 "body" is coated by one (or several) Cu "caps", as evident by EDS (Fig. 5e). These results indicate that further formulation optimization could be done to reduce the reactive sintering of Al-CuO to further enhance the reactivity.

4. Conclusion

We have prepared a colloidal ink with 90 wt% Al-CuO and 10 wt% hybrid polymers that enables one to print mechanically strong and highly reactive materials, that operationally behave like a dense thermite powder compact. We believe that the in-situ production of PS flakes is an important component in establishing the mechanical integrity of the materials, while still maintaining combustion performance. This approach was shown to be generic as evidenced by similar behavior with three other oxidizers. This study offers an attractive route for safe, reliable and scalable additive manufacturing of Al-based nano-energetic materials.

Declaration of Competing Interest

There is no conflict of interest.

Acknowledgments

This work was supported by the AFOSR. We acknowledge the support of the Maryland Nanocenter and its NispLab. The NispLab is supported in part by the NSF as an MRSEC Shared Experimental Facility. Supporting Information is available online from journal website or from the authors. J. Shen would like to acknowledge the China Scholarship Council (CSC) for financial support.

Supplementary materials

Supplementary material associated with this article can be found, in the online version, at doi:10.1016/j.combustflame.2020.01.021.

References

[1] D. Sundaram, V. Yang, R.A. Yetter, Metal-based nanoenergetic materials: synthesis, properties, and applications, Prog. Energy Combust. Sci. 61 (2017) 293–365.
[2] W. He, P. Liu, G. He, Gozin M, Q.L. Yan, Highly reactive metastable intermixed composites (MICs): preparation and characterization, Adv. Mater. (2018) 1706293.
[3] M.R. Zachariah, Nanoenergetics: hype, reality and future, Propellants Explos. Pyrotech. 38 (2013) 7.
[4] C. Wu, K. Sullivan, S. Chowdhury, G. Jian, L. Zhou, M.R. Zachariah, Encapsulation of perchlorate salts within metal oxides for application as nanoenergetic oxidizers, Adv. Funct. Mater. 22 (2012) 78–85.
[5] G. Jian, L. Liu, M.R. Zachariah, Facile aerosol route to hollow CuO spheres and its superior performance as an oxidizer in nanoenergetic gas generators, Adv. Funct. Mater. 23 (2013) 1341–1346.
[6] E.L. Dreizin, Metal-based reactive nanomaterials, Prog. Energy Combust. Sci. 35 (2009) 141–167.
[7] S.S. Pandey, N. Banerjee, Y. Xie, C.H. Mastrangelo, self-destructing secured microchips by on-chip triggered energetic and corrosive attacks for transient electronics, Adv. Mater. Technol. (2018) 1800044.

[8] E.L. Dreizin, M. Schoenitz, Correlating ignition mechanisms of aluminum-based reactive materials with thermoanalytical measurements, Prog. Energy Combust. Sci. 50 (2015) 81–105.
[9] A. Varma, A.S. Rogachev, A.S. Mukasyan, S. Hwang, Complex behavior of self-propagating reaction waves in heterogeneous media, Proc. Natl. Acad. Sci. USA. 95 (1998) 11053–11058.
[10] G.C. Egan, M.R. Zachariah, Commentary on the heat transfer mechanisms controlling propagation in nanothermites, Combust. Flame 162 (2015) 2959–2961.
[11] G.C. Egan, T. LaGrange, M.R. Zachariah, Time-resolved nanosecond imaging of nanoscale condensed phase reaction, J. Phys. Chem. C 119 (2015) 2792–2797.
[12] R.J. Jacob, G. Jian, P.M. Guerieri, M.R. Zachariah, Energy release pathways in nanothermites follow through the condensed state, Combust. Flame 162 (2015) 258–264.
[13] J. Shen, Z. Qiao, J. Wang, G. Yang, J. Chen, Z. Li, X. Liao, H. Wang, M.R. Zachariah, Reaction mechanism of Al-CuO nanothermites with addition of multilayer Graphene, Thermochim. Acta 666 (2018) 60–65.
[14] K.B. Plantier, M.L. Pantoya, A.E. Gash, Combustion wave speeds of nanocomposite Al/Fe_2O_3: the effects of Fe_2O_3 particle synthesis technique, Combust. Flame 140 (2005) 299–309.
[15] T.M. Tillotson, A.E. Gash, R.L. Simpson, L.W. Hrubesh, J.H. Satcher, J.F. Poco, Nanostructured energetic materials using sol-gel methodologies, J. Non-Cryst. Solids 285 (2001) 338–345.
[16] M. Schoenitz, T.S. Ward, E.L. Dreizin, Fully dense nano-composite energetic powders prepared by arrested reactive milling, Proc. Combust. Inst. 30 (2005) 2071–2078.
[17] M. Petrantoni, C. Rossi, L. Salvagnac, V. Conedéra, À. Estéve, C. Tenailleau, P. Alphonse, Y.J. Chabal, Multilayered Al/CuO thermite formation by reactive magnetron sputtering: nano versus micro, J. Appl. Phys. 108 (2010) 084323.
[18] A.H. Kinsey, K. Slusarski, S. Sosa, T.P. Weihs, Gas suppression via copper interlayers in magnetron sputtered Al-Cu_2O multilayers, ACS Appl. Mater. Interfaces 9 (2017) 22026–22036.
[19] H.Y. Wang, G.Q. Jian, G.C. Egan, M.R. Zachariah, Assembly and reactive properties of Al/CuO based nanothermite microparticles, Combust. Flame 161 (2014) 2203–2208.
[20] F. Séverac, P. Alphonse, A. Estève, A. Bancaud, C. Rossi, Assembly and reactive properties of Al/CuO based nanothermite microparticles, Adv. Funct. Mater. 22 (2012) 323–329.
[21] W. He, P. Liu, F. Gong, B. Tao, J. Gu, Z. Yang, Q. Yan, Tuning the reactivity of metastable intermixed composite n-Al/PTFE by polydopamine interfacial control, ACS Appl. Mater. Interfaces 10 (2018) 32849–32858.
[22] J. Lyu, S. Chen, W. He, X. Zhang, D. Tang, P. Liu, Q. Yan, Fabrication of high-performance graphene oxide doped PVDF/CuO/Al nanocomposites via electrospinning, Chem. Eng. J. 368 (2019) 129–137.
[23] W. He, Z. Li, S. Chen, G. Yang, Z. Yan, P. Liu, Q. Yan, Energetic metastable n-Al@PVDF/EMOF composite nanofibers with improved combustion performances, Chem. Eng. J. 383 (2020) 123146.
[24] W. He, W. Ao, G. Yang, Z. Yang, Z. Guo, P. Liu, Q. Yan, Metastable energetic nanocomposites of MOF-activated aluminum featured with multi-level energy releases, Chem. Eng. J. 381 (2020) 122623.
[25] D.A. Wiegand, S. Nicolaides, J. Pinto, Mechanical and thermomechanical properties of NC base propellants, J. Energetic Mater. 8 (1990) 442–461.
[26] S. Apte, V. Yang, Unsteady flow evolution and combustion dynamics of homogeneous solid propellant in a rocket motor, Combust. Flame 131 (2002) 110–131.
[27] J. Shen, Z. Liu, B. Xu, H. Liang, Y. Zhu, X. Liao, Z. Wang, Influence of carbon nanofibers on thermal and mechanical properties of NC-TEGDN-RDX triple-base gun propellants, Propellants Explos. Pyrotech. 44 (2019) 355–361.
[28] H. Yuk, X. Zhao, A new 3D printing strategy by harnessing deformation, instability, and fracture of viscoelastic inks, Adv. Mater. 30 (2018) 1704028.
[29] E.B. Duoss, T.H. Weisgraber, K. Hearon, C. Zhu, W. Small, T.R. Metz, J.J. Vericella, H.D. Barth, J.D. Kuntz, R.S. Maxwell, Three-dimensional printing of elastomeric, cellular architectures with negative stiffness, Adv. Funct. Mater. 24 (2014) 4905–4913.
[30] Y. Yang, X. Li, X. Zheng, Z. Chen, Q. Zhou, Y. Chen, 3D-printed biomimetic super-hydrophobic structure for microdroplet manipulation and oil/water separation, Adv. Mater. 30 (2018) 1704912.
[31] H. Kang, S.J. Lee, I.K. Ko, C. Kengla, J.J. Yoo, A. Atala, A 3D bioprinting system to produce human-scale tissue constructs with structural integrity, Nat Biotechnol. 34 (2016) 312–319.
[32] J.S. Miller, K.R. Stevens, M.T. Yang, B.M. Baker, D.-H.T. Nguyen, D.M. Cohen, E. Toro, A.A. Chen, P.A. Galie, X. Yu, Rapid casting of patterned vascular networks for perfusable engineered three-dimensional tissues, Nat. Mater. 11 (2012) 768–774.
[33] B.Y. Ahn, E.B. Duoss, M.J. Motala, X. Guo, S.-I. Park, Y. Xiong, J. Yoon, R.G. Nuzzo, J.A. Rogers, J.A. Lewis, Omnidirectional printing of flexible, stretchable, and spanning silver microelectrodes, Science 323 (2009) 1590–1593.
[34] L.S. Dimas, G.H. Bratzel, I. Eylon, M.J. Buehler, Tough composites inspired by mineralized natural materials: computation, 3D printing, and testing, Adv. Funct. Mater. 23 (2013) 4629–4638.
[35] K. Tian, J. Bae, S.E. Bakarich, C. Yang, R.D. Gately, G.M. Spinks, Z. Suo, J.J. Vlassak, 3D printing of transparent and conductive heterogeneous hydrogel-elastomer systems, Adv. Mater. 29 (2017) 1604827.
[36] C. Xu, C. An, Y. He, Y. Zhang, Q. Li, J. Wang, Direct ink writing of DNTF based composite with high performance, Propellants Explos. Pyrotech. 43 (2018) 754–758.
[37] Q. Li, C. An, X. Han, C. Xu, C. Song, B. Ye, B. Wu, J. Wang, CL-20 based explosive ink of emulsion binder system for direct ink writing, Propellants Explos. Pyrotech. 43 (2018) 533–537.
[38] D. Wang, B. Zheng, C. Guo, B. Gao, J. Wang, G. Yang, H. Huang, F. Nie, Formulation and performance of functional sub-micro CL-20-based energetic polymer composite ink for direct-write assembly, RSC Adv. 6 (2016) 112325.
[39] R.A. Chandru, N. Balasubramanian, C. Oommen, B.N. Raghunandan, Additive manufacturing of solid rocket propellant grains, J. Propul. Power 34 (2018) 1090–1093.
[40] C. van Driel, M. Straathof, J. van Lingen, Developments in additive manufacturing of energetic materials at TNO, The 30th International Symposium on Ballistics, Long Beach (2017).
[41] A.K. Murray, W.A. Novotny, T.J. Fleck, I.E. Gunduz, S.F. Son, G.T.-C. Chiu, J.F. Rhoads, Selectively-deposited energetic materials: a feasibility study of the piezoelectric inkjet printing of nanothermites, Addit. Manuf. 22 (2018) 69–74.
[42] J.M. Slocik, R. McKenzie, P.B. Dennis, R.R. Naik, Creation of energetic biothermite inks using ferritin liquid protein, Nat. Commun. 8 (2017) 15156.
[43] M.M. Durban, A.M. Golobic, E.V. Bukovsky, A.E. Gash, K.T. Sullivan, Development and characterization of 3D printable thermite component materials, Adv. Mater.Technol. 3 (2018) 1800120.
[44] H. Wang, J. Shen, D.J. Kline, N. Eckman, N.R. Agrawal, T. Wu, P. Wang, M.R. Zachariah, Direct writing of a 90 wt% particle loading nanothermite, Adv. Mater. (2019) 1806575.
[45] J. Hübner, M. Klaumünzer, M. Comet, C. Martin, L. Vidal, M. Schäfer, C. Kryschi, D. Spitzer, Insights into combustion mechanisms of variable aluminum-based iron oxide/-hydroxide nanothermites, Combust. Flame 184 (2017) 186–194.
[46] K.T. Sullivan, N.W. Piekiel, C. Wu, S. Chowdhury, S.T. Kelly, T.C. Hufnagel, K. Fezzaa, M.R. Zachariah, Reactive sintering: an important component in the combustion of nanocomposite thermites, Combust. Flame 159 (2012) 2–15.
[47] K.T. Sullivan, J.D. Kuntz, A.E. Gash, The role of fuel particle size on flame propagation velocity in thermites with a nanoscale oxidizer, Propellants Explos. Pyrotech. 39 (2014) 407–415.
[48] N. Zohari, M.H. Keshavarz, S.A. Seyedsadjadi, The advantages and shortcomings of using nano-sized energetic materials, Cent. Eur. J. Energ. Mat. 10 (2013) 135–147.
[49] P. Chakraborty, M.R. Zachariah, Do nanoenergetic particles remain nano-sized during combustion? Combust. Flame 161 (2014) 1408–1416.
[50] H. Wang, D.J. Kline, M.R. Zachariah, In-operando high-speed microscopy and thermometry of reaction propagation and sintering in a nanocomposite, Nat. Commun. 10 (2019) 3032.
[51] R.J. Jacob, D.J. Kline, M.R. Zachariah, High speed 2-dimensional temperature measurements of nanothermite composites: probing thermal vs. gas generation effects, J. Appl. Phys. 123 (2018) 115902.
[52] F. Fallah, M. Khorasani, M. Ebrahimi, Improving the mechanical properties of waterborne nitrocellulose coating using nano-silica particles, Progress. Org. Coat. 109 (2017) 110–116.
[53] W.T. Hay, G.F. Fanta, S.C. Peterson, A.J. Thomas, K.D. Utt, K.A. Walsh, V.M. Boddu, G.W. Selling, Improved hydroxypropyl methylcellulose (HPMC) films through incorporation of amylose-sodium palmitate inclusion complexes, Carbohyd. Polym. 188 (2018) 76–84.
[54] I. Oral, H. Guzel, G. Ahmetli, Measuring the Young's modulus of polystyrene-based composites by tensile test and pulse-echo method, Polym. Bull. 67 (2011) 1893–1906.
[55] J.T. Muth, D.M. Vogt, R.L. Truby, Y. Mengüç, D.B. Kolesky, R.J. Wood, J.A. Lewis, Embedded 3D printing of strain sensors within highly stretchable elastomers, Adv. Mater. 26 (2014) 6307–6312.
[56] L. Xu, X. Zhao, C. Xu, N.A. Kotov, Water-rich biomimetic composites with abiotic self-organizing nanofiber network, Adv. Mater. 30 (2018) 1703343.
[57] X. Li, P. Guerieri, W. Zhou, C. Huang, M.R. Zachariah, Direct deposit laminate nanocomposites with enhanced propellent properties, ACS Appl. Mater. Interfaces 7 (2015) 9103–9109.
[58] H. Wang, S. Holdren, M.R. Zachariah, Preparation and combustion of laminated iodine containing aluminum/polyvinylidene fluoride composites, Combust. Flame 197 (2018) 120–126.
[59] H. Wang, D.J. Kline, M. Rehwoldt, T. Wu, W. Zhao, X. Wang, M.R. Zachariah, Architecture can significantly alter the energy release rate from nanocomposite energetics, ACS Appl. Polym. Mater. 1 (2019) 982–989.
[60] J.L. Murray, The aluminium-copper systemInt, Met. Rev. 30 (1985) 211–234.
[61] L. Zhou, N. Piekiel, S. Chowdhury, M.R. Zachariah, Time-resolved mass spectrometry of the exothermic reaction between nanoaluminum and metal oxides: the role of oxygen release, J. Phys. Chem. C 114 (2010) 14269–14275.
[62] V.E. Sanders, B.W. Asay, T.J. Foley, B.C. Tappan, A.N. Pacheco, S.F. Son, Reaction propagation of four nanoscale energetic composites (Al/MoO3, Al/WO3, Al/CuO, and Bi2O3), J. Propul. Power 23 (2007) 707–714.
[63] H. Wang, G. Jian, W. Zhou, J.B. DeLisio, V.T. Lee, M.R. Zachariah, Metal iodate-based energetic composites and their combustion and biocidal performance, ACS Appl. Mater. Interfaces 7 (2015) 17363–17370.